Desalination and Water Treatment
www.deswater.com
doi: 10.5004/dwt.2020.25781

192 (2020) 259–270
July

Isotherm and kinetic studies for adsorption of boron on nano-copper oxide (CuO) in non-competitive and competitive solutions

Shahriar Mahdavi*, Zahra Salehi, Mahboubeh Zarabi

Department of Soil Science, Faculty of Agriculture, Malayer University, Malayer, Iran, Tel./Fax: +98 8132355338; emails: smahdaviha@yahoo.com/sh.mahdavi@malayeru.ac.ir (S. Mahdavi), salehizahra13@yahoo.com (Z. Salehi), zarrabi7@gmail.com (M. Zarabi)

Received 24 July 2019; Accepted 4 March 2020

ABSTRACT

In this work, the effects of temperature, time, and adsorbate initial concentrations were investigated on the adsorption efficiency of Cooper oxide (CuO) nanoparticles (NPs) as the adsorbent of boron. In addition, surface properties of CuO were examined using the power X-ray diffraction, specific area by Brunauer–Emmett–Teller method, scanning electron microscopy – energy dispersive X-ray, Fourier transform infrared, and point of zero charge (PZC). Our careful scientific examination action revealed that CuO had very small particles with a mean diameter of 85 nm. Subsequent experiments showed that the adsorption of boron needed neither acidic nor alkaline pH (pH = 7) at temperatures 25°C. Moreover, positive values of $\Delta H°$ suggested that the reaction was endothermic whereas negative values for $\Delta G°$ showed that adsorption processes were spontaneous. According to the kinetic studies the data better fitted to pseudo-second-order rather than first order. Under the best condition, the CuO adsorption capacity was 3.5 mg/g in a non-competitive solution. However, the amounts of B removal in CuO NPs were 3.0, 3.0, 3.5, and 2.8 mg/g by existing competitive anions, namely humate, phosphate, sulfate, and citrate, respectively. Linear Freundlich among Freundlich, Langmuir, Temkin, and Dubininn and Radushkevich (D–R) models could be considered as the best model in order to explain experimental data with a high average coefficient of determination (R^2 = 0.9628). The results indicated that CuO NPs can be considered a promising adsorbent for water purification due to its efficiency in removing boron.

Keywords: CuO nanoparticles; Boron; Isotherm; Water

1. Introduction

According to geological surveys (2012), it was found that less than 3% of the whole water is useable on the earth. Therefore, lots of attempts have been carried out to improve some technologies to have extra freshwater from streams of unusable waters such as seawater, salty, non-pure water, and wastewater [1]. Boron is one of the drinking water pollutants that has negative effects on living organisms [2]. It is a trace element, divided broadly in hydrosphere and lithosphere, and its average concentration in the hydrosphere is around 4.5 mg/L in seawater whereas the concentration differs from 0.3 to 100 mg/L in groundwater [3]. Boron contamination in the environment still is increasing due to different natural sources and anthropology works. For many years, a limit of 0.3 mg/L was set for boron in drinking water by the World Health Organization, however, this amount changed to 2.4 mg/L in 2011 owing

* Corresponding author.

to the impressive effect of boron on the health of people. On the contrary, the EU still offers the highest boron concentration (1.0 mg/L) in drinking water. Consequently, removing B from water became a worldwide harsh situation because of its continuous poisonous effect on plants, animals, and human health [4]. Unlike most of the elements dissolved in water and seawater, B is not easily ionized (i.e. it has no charge) but is present in water and seawater as boric acid, $B(OH)_3$, and as borate at high pH (9.2). The existence of B affects directly the pH of the water. In the seawater with a pH of about 8, $B(OH)_3$ is going to increase [5].

Two wide classified groups are determined to remove B from wastewater, namely (1) dividing by adsorption on solid, and (2) dividing by membrane filtration. Precipitation–coagulation, adsorption (with clays and nanoparticles), chemical precipitation, ion exchange (with resins), biosorption, reverse osmosis, ultra-filtration or nano-filtration, electrochemical methods, thermal methods, and evaporation–crystallization processes are some cases for sorption by solids and filtration [1,5–9]. On the other hand, both general methods have their own application limits, both of which are mostly limited because of technical and economic issues. Among reported methods for B removal, adsorption was one of the most observed processes because of high adsorption capacity, easy operability, remarkable recycling performance, and relatively low cost [10]. Thus, the removal of boron has been reported using various adsorbents, such as commercial activated carbons (CACs) [11], polymeric resin [12], waste tire rubber [13], oxides and hydroxides [3], Fe_3O_4 [10], and date palm seed ash [5]. Recent findings show that nanoparticles (NPs) have highly promising adsorption due to their affinities towards impurities and higher surface area per unit volume. Therefore, nanoparticles have nowadays attracted a lot of attention in order to clean the environment from pollutants [6,14–16].

Among different types of nanoparticles, copper oxide (CuO) NPs are widely used as *p*-type narrow band gap semiconductors (E_{gap} = 1.0–2.08 eV) in various applications such as gas sensors, lithium ion electrode materials, magnetics, and photocatalysts; due to their abundance and low cost, they are also effective adsorbents for the removal of metal ions and anions, as well as dyes such as phosphate, chromate, and Methylene blue from wastewater. However, no report can yet be found on the utilization of CuO NPs for removal of B from water [15,17–22]. Simultaneously, the relatively high value of pH_{PZC} (9.4) permits the removal of anionic species at a higher pH range typical for natural waters due to electrostatic attraction of negatively charged arsenic species and positively charged cupric oxide surface [23].

The purpose of the present work was to use engineered CuO NPs for the removal of B from non-competitive and competitive (sulfate, phosphate, citrate, and humate anions) solutions. Thereafter, X-ray diffraction (XRD), scanning electron microscope – energy dispersive X-ray (SEM-EDX), Brunauer–Emmett–Teller (BET), and Fourier transform infrared (FTIR) techniques were used to characterize bare CuO NPs to be used as an adsorbent for the removal of B ions through adsorption. The B adsorbability of novel CuO NPs was examined through different batch adsorption experiments such as pH, dose of adsorbent, contact time (kinetics), temperature (thermodynamic parameters), and adsorbent concentration effects. Finally, isotherm experiments and isotherm models were studied on CuO NPs to obtain sorption capacities, as well as SEM-EDX analysis and desorption experiments for better understanding of sorption mechanisms after doing isotherm experiments.

2. Materials and methods

2.1. Materials and technical and instrumental analysis

All kinds of chemical material, such as H_3BO_3, K_2SO_4, KH_2PO_4, Humic acid, and $Na_3C_6H_5O_7$, used here were classified on analytical grade. All mentioned materials were procured from Merck Co. Ltd., (Germany) and Sigma-Aldrich (USA). The CuO NPs (99.0% purity) were taken from Nabond Ltd., China. All stock and fresh solutions were made with deionized water. Boron was measured spectrophotometrically at 420 nm wavelength by the Azomethine methods (WPAS2000 spectrophotometer) [24]. The crystal phase of the CuO NPs was detected on an X-ray diffractometer (XRD-Unisantis, Germany) acted at 40 kV and 30 mA with Cu/Ka radiation having a 2θ ranging from 0 to 80. The morphology of the CuO NPs was evaluated by a scanning electron microscope associated with energy dispersive X-ray (SEM-EDX, Tscan Company, Czech). The BET specific surface area and pore volume established from as N_2 adsorption/desorption isotherms were determined using an automated nitrogen adsorption analyzer (BEL, Belsorp mini II, Japan). The CuO NPs functional groups were detected by a Perkin–Elmer spectrum (USA) Fourier transform infrared (FTIR) spectrometer with a potassium bromide (KBr) method. Analyzed spectra were in the range of 400–4,000 cm^{-1}. The pH at the point of zero charge (pH_{PZC}) of copper oxide nanoparticles was measured by the pH drift method [21].

2.2. Adsorption procedure

Adsorption experiments were carried out using a batch system. The effects of pH level, temperature, time, and adsorbent dosage on B removal were evaluated through a group of particular sorption studies (optimization experiments). A pH value between 3.0 and 8.0 was synthesized in pH experiments. Besides, an adsorbent dosage of 1 g/L (25 mg of CuO NPs at 25 ml B solution), constant concentration of 10 mg B/L, 25°C, and an equilibrium time of 24 h were used in 50 mL falcon tubes. The experiments of adsorbent dosage were performed with 0.5, 1, 1.5, 2, 2.5, and 3 g/L of CuO NPs and a constant concentration of 10 mg B/L, native pH, 25°C, and an equilibrium time of 24 h in 50 mL falcon tubes. The temperature effect was designed at 15, 20°C, 25°C, 30°C, 35°C, and 40°C with the same parameters of the adsorbent dosage section. The time effect parameters were studied from 10 to 180 min, and the other parameters were the same as the adsorbent dosage section. B solution and the adsorbent were shaken at 100 rpm mixing rate in a mechanical shaker. At the end of each experiment, the suspension was centrifuged and filtered through a 0.22 μm filter. The filtrate was measured for B concentration by the Azomethine-H method [24]. All sorption tests were done for three times to reach the average and similar consequences. At the end, B adsorption coefficients (the removal efficiency, *R* [%], and the adsorptive

capacity, q [mg/g]) were calculated from the experimental data for each sample using the following equations:

$$R(\%) = \frac{C_0 - C}{C_0} \times 100 \quad (1)$$

$$Q = \frac{C_0 - C}{m} \times V_0 \quad (2)$$

where C_e (mg L^{-1}) and C_0 (mg L^{-1}) are instant B concentration and initial B concentration, respectively, while C_0 (L) and m (g) represented the volume of solution and the amount of added NPs (CuO), respectively.

Optimum parameters from each section were used in the isotherm experiment in order to design the isotherm models and adsorption capacity of CuO NPs.

2.3. Kinetic and thermodynamic parameters

The situation mechanism of the sorption was shown using kinetic models. The careful attention of the adsorption mechanism was specified using three broadly applied kinetic models. The models, viz. pseudo-first-order (PFO), pseudo-second-order (PSO), and intraparticle diffusion (IP) were employed for modeling the adsorption process. Table 1 shows the non-linear and linear equations along with constants regarding these kinetic models. The k_1 (1/min) and k_2 (mg/g min) are the rate coefficients for PFO and PSO kinetic models, respectively. Also, q_e and q_t (mg/g) are the adsorption capacities at equilibrium and at time t, respectively. As reported in the literature, the IP model is mostly utilized to figure out the adsorption process mechanism. K_{IP} (mg/g $min^{0.5}$) is the constant rate of the IP, and C_{IP} (mg/g) is the constant explaining the boundary layer effects [17,25]. The thermodynamic parameters, such as Gibb's free energy change ($\Delta G°$), enthalpy change ($\Delta H°$), and entropy change ($\Delta S°$) for the adsorption process, were calculated by Eqs. (4) and (5) [21,26].

$$K_c = \frac{q_e}{C_e} \quad (3)$$

$$\Delta G° = -RT \ln K_c \quad (4)$$

$$\Delta G° = \Delta H° - T\Delta S° \quad (5)$$

where K_c is the equilibrium constant resulting from the ratio of the equilibrium adsorbed concentrations of B (q_e) on CuO NPs and equilibrium concentration in solution (C_e), R is the ideal gas constant (8.314J/mol/K), and T is the temperature in Kelvin. The values of $\Delta G°$ were calculated by understanding the values of K_C, and the values of $\Delta H°$ and $\Delta S°$ were measured from the intercept and slope of the $\Delta G°$ vs. T plot.

2.4. Adsorption isotherms in competitive and non-competitive solutions

The relationship between the amounts of ions adsorbed and the ions concentration remaining in the solution is depicted by an isotherm [9]. The sorption isotherms were obtained at pH 7 by changing the initial B concentration (2, 4, 6, 8, and 10 mg/L). In each test, 25 mL solution with different B concentrations was added into a 50 mL falcon tube, and then 37.5 mg of the sorbent sample was dosed into the tube (1.5 g/L). The solutions were shaken at a constant 25°C for 90 min. After filtration with 0.22 μm membrane filters, the residual B concentration was determined, followed by calculating the amount of B adsorbed by CuO NPs. The concentrations of coexisting anions (phosphate, humate, citrate, and sulfate) were equal to that of boron at each point. A sorbent amount of 1.5 g/L (3.75 mg sorbent in 25 mL solution) was added into tubes and shaken for 90 min. Then, water samples were filtrated by 0.22 μm membrane filters and the residual concentrations of B were determined in the filtrates.

2.5. Desorption and regeneration studies

For desorption studies, the adsorption was first performed in isotherm experiments (with competitive and non-competitive solutions in a B concentration of 2mg/L) ,and then washed with distilled water. CuO NPs bearing adsorbed B ions were collected and gently washed with distilled water. The obtained CuO NPs were then added to 25 mL of $CaCl_2$ (0.01 M) solution (with an equilibrium time of 24 h) and the desorbed B ion concentrations were determined via supernatant analysis using a spectrophotometric apparatus through the Azomethine-H method

Table 1
Constants and equations of kinetic and isotherm models studied for B adsorption onto CuO NPs

Kinetic/isotherm model	Equation	Linear equation	Plot	Parameters
Kinetic models				
Pseudo-first-order	$dq_t/d_t = k_1 (q_e - q_t)$	$\ln(q_e - q_t) = \ln q_e - k_1 t$	$\ln(q_e - q_t)$ vs. t	q_e (mg/g), k_1 (min^{-1})
Pseudo-second-order	$dqt/dt = k_2 (q_e - q_t)^2$	$t/q_t = t/q_e + 1/k_2 q_e^2$	t/q_t vs. t	q_e (mg/g), k_2 (mg/g min)
Intra-particle diffusion	$q_t = k_{ip} t^{0.5} + C_{ip}$	$q_t = k_{ip} t^{0.5} + C_{ip}$	q_t vs. $t^{0.5}$	k_{ip} (mg/g $min^{0.5}$), C_{ip} (mg/g)
Isotherm models				
Freundlich	$q_e = K_F (C_e)^{1/n}$	$\ln q_e = \ln K_F + n^{-1} \ln C_e$	$\ln q_e$ vs. $\ln C_e$	K_F (mg/g(L mg)$^{1/n}$), n
Langmuir	$q_e = (q_m K_L C_e)/(1 + K_L C_e)$	$C_e/q_e = C_e/q_m + 1/K_L q_m$	(C_e/q_e) vs. C_e	q_m (mg/g), K_L (L/mg)
Temkin	$q_e = B \ln(K_T C_e)$	$q_e = B \ln K_T + B \ln C_e$	q_e vs. $\ln C_e$	B (mg/g), K_T
Dubbin–Raduashkevich (D–R)	$\ln q_e = \ln q_m - \varepsilon^2 \beta$		ε^2 vs. q_e	q_m (mg/g), β (mol²/kJ²)

[25]. The desorption ratios of B ions from CuO NPs were deduced from the amounts of ions adsorbed before and after the desorption step.

3. Results and discussion

3.1. Characterization of CuO NPs

The SEM image of prepared CuO nanoparticles (Fig. 1) shows irregularly sized particles with an average diameter of 85 nm. High porosity of particles is also clearly revealed in the morphology of the CuO NPs (Fig. 1). Fig. 2 displays the EDX spectra of the CuO NPs, with an appropriate stoichiometric ratio of Cu and O (1:1), which stabilizes the formation of pure CuO nanoparticles. FTIR is commonly used to investigate functional groups. Fig. 3 presents the FTIR spectra of CuO nanoparticles, with a peak at 522.53 cm^{-1} indicating the formation of the monoclinic CuO phase [15]. The peaks of all the samples were represented at 3,425.37 and 1,632.59 cm^{-1}, corresponding to the stretching vibration of the surface hydroxyl groups (OH) and bending vibration of the adsorbed water (H_2O), respectively [24]. The peak around 1,117.74 cm^{-1} (Fig. 3) should be ascribed to O–H bending vibrations combined with CuO atoms [15,27]. The XRD patterns of CuO NPs (Fig. 4) reveal that the CuO is crystalline in nature. The spectrum is similar to that of pure CuO, indicating the formation of single-phase CuO with monoclinic structure (JCPDS–05–0661). In the present work, diffraction patterns observed to be at 2θ = 32.5, 35.5, 38.7, 48.6, 53.4, 58.2, and 61.4 were assigned to the reflection lines of monoclinic CuO NPs. The present experimental results are in agreement with the reported diffraction patterns of CuO NPs prepared by Padil and Cernik [28]. The peaks obtained in the XRD pattern explain the formation of a high purity phase of the CuO NPs, as there is no peak of any impurity in the XRD pattern. The particle size (~59.4 nm) was further estimated by selecting the main diffraction using the Scherer formula, which is not in good agreement with the SEM results [21]. The BET surface area, the BJH average pore size, and the BJH pore volume of the CuO NPs are 12.1 m^2/g, 54.1 nm, and 3.15 × 10^{-2} cm^3/g, respectively (Table 2).

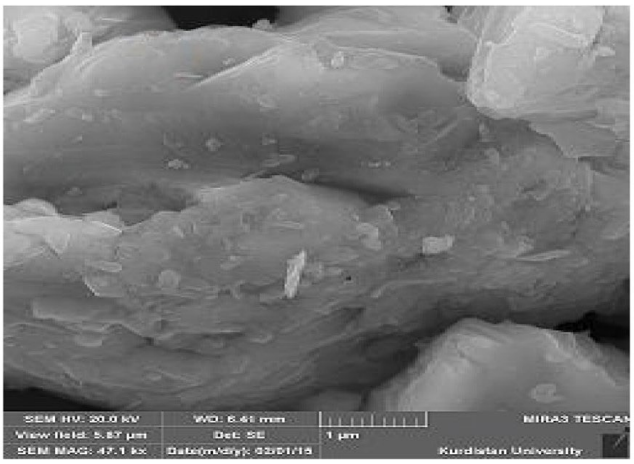

Fig. 1. SEM image of CuO NPs.

3.2. Effects of solution pH/temperature on boron removal

pH value is the main factor for the optimization of the sorption mechanism process because the interposition of protons with the sorbent may affect the efficiency of the material. The effect of the solution pH on the efficiency of B removal was measured in batch experiments at a constant temperature of 25°C, B concentration of 10mg/L, and CuO dosage of 1 g/L. As shown in Fig. 5, the maximum sorption was gained at pH 7 with a removal efficiency of 33.7%. The lowest B removal efficiency, on the other hand, was earned at pH 3. Because the PZC of CuO NPs is 8 (Table 2), and at the acidic conditions (pH < 7), boric acid is the predominant B species, thus the adsorption appears to be specific or chemical sorption. However, part of the adsorption is also dependent on pH [29,30]. The temperature dependence adsorption and its thermodynamic were studied at six different temperatures (15°C, 20°C, 25°C, 30°C, 35°C, and 45°C)

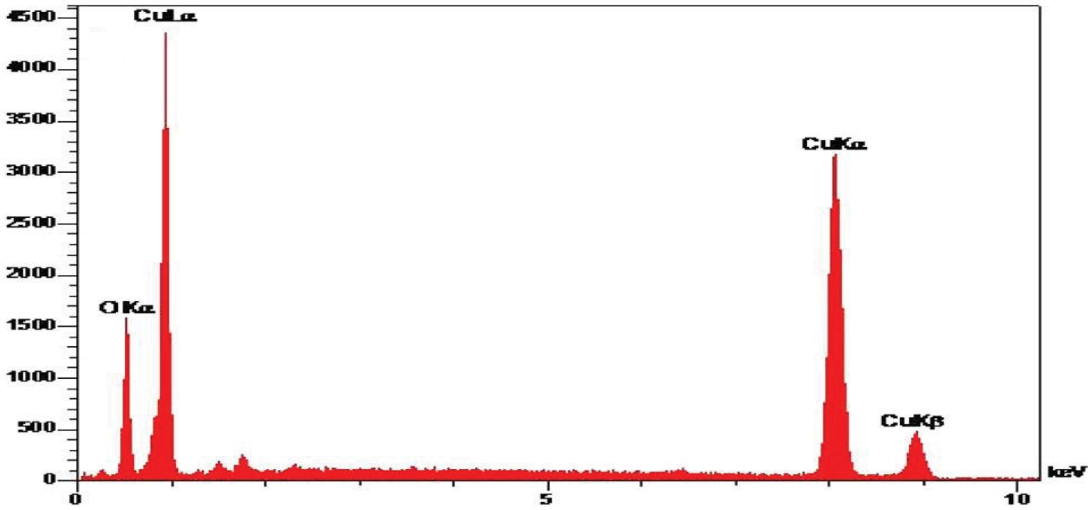

Fig. 2. EDX spectra of CuO.

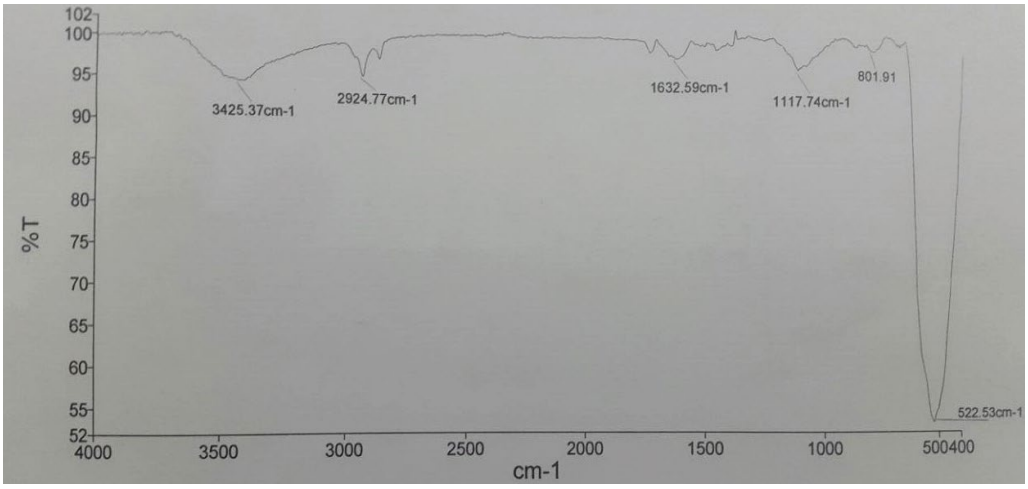

Fig. 3. FTIR analysis of CuO nanoparticles indicating the involvement of various functional groups in the formation of metal oxide nanoparticles.

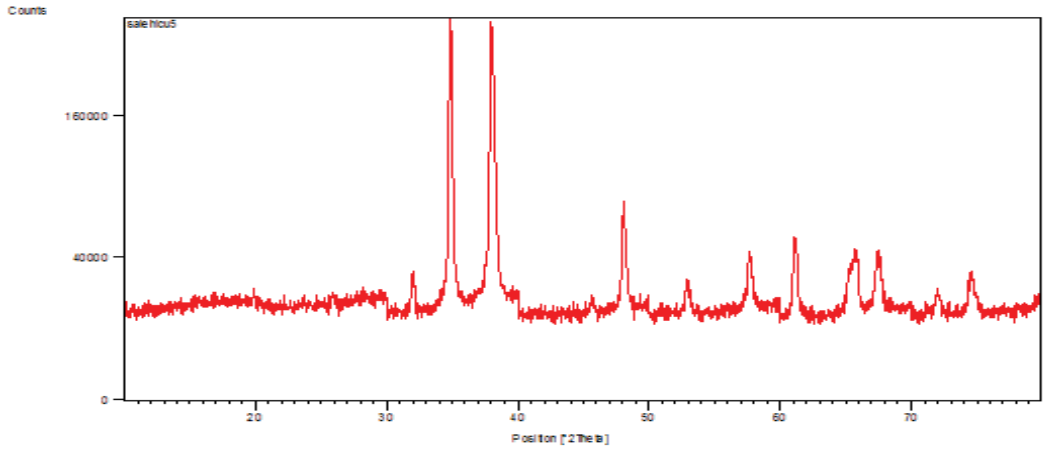

Fig. 4. Pattern of synthesized CuO NPs.

Table 2
Properties of CuO nanoparticles

Nanoparticle	CuO
Particle size, nm	85.0
Crystal size, nm	59.4
ZPC	8.0
BET, m^2/g	12.1
Pore volume, cm^3/g	3.15×10^{-2}
Pore size nm	54.1

on CuO NPs based adsorbent, while all the other parameters, such as adsorbent dose (1.0 g/L), B ions concentration (10 mg/L), and contact time (24 h), were fixed manually at optimized levels. The results showed that with an increase in the temperature from 15 to 45°C, the percentage adsorption of B ions increased from 37.1% to 45.0%. The thermodynamic parameters, such as Gibb's free energy change ($\Delta G°$), enthalpy change ($\Delta H°$), and entropy ($\Delta S°$), were calculated using Eqs. (4) and (5) (Table 3). The negative free energy changes ($\Delta G°$) revealed that the adsorption of B onto CuO NPs was possible and spontaneous thermodynamically. The positive value of $\Delta H°$ further demonstrates that the adsorption was an endothermic process and could be classified into physisorption since all the $\Delta H°$ values fall lower than 20.9 kJ/mol [31,32]. The positive $\Delta H°$ is unfavorable for spontaneous adsorption, while the positive $\Delta S°$ is favorable for spontaneous adsorption. Therefore, the driving force for the B adsorption on CuO is controlled by an entropy effect rather than an enthalpy change [17,33].

3.3. Effect of CuO NPs dosage and contact time on B removal

B removal increased to some extent with an increase in the CuO NPs dosage (Fig. 6). The larger B uptake with the CuO dosage is explained by an increased total surface area and a number of binding sites on the CuO surfaces. Fig. 6 shows the plot between the removal of B ions and

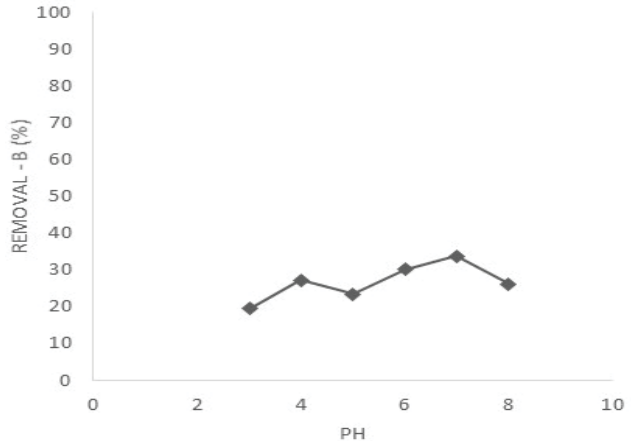

Fig. 5. Effect of pH on B adsorption on CuO NPs; C_0 = 10 mg/L, sorbent dosage (SD): 1.0 g/L, and t = 24 h.

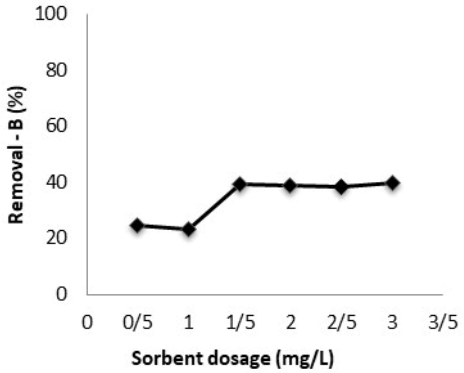

Fig. 6. Effect of adsorbent dose (adsorbent dose varied in a range of 0.5–3.5 mg/L and the initial B ions concentration of 10 mg/L was used at 25°C).

adsorbent dose. As it is clear, B ions removal rose sharply from 24.8% to 39.4% as the adsorbent dose increased from 0.5 to 1.5 g/L, but there was no further increase with higher adsorbent doses of 2–3.5 g/L. On the other hand, the adsorption capacity of CuO NPs decreased gradually from 4.95 to 1.32 mg/g with an increase in the adsorbent dose (10 mg/L) relative to the initial concentration of B ions. In fact, the adsorption capacity of the adsorbent depends upon the ions to binding sites ratio. At higher doses, the available B ions were insufficient to saturate the entire binding sites existing on CuO NPs surfaces, thus resulting in less adsorption of B ions on per unit weight of CuO NPs, thereby lowering the adsorption capacity. In addition, the removal of B ions increases due to sufficient availability of large surface areas and vacant adsorption sites at higher adsorbent doses. At the equilibrium state, a further increase in the adsorbent dose resulted in a slight enhancement in the removal of B ions. Therefore, a dosage of 1.5 g/L was used for further experiments to maintain the reasonable values of high removal efficiency and adsorption capacity per unit mass of CuO adsorbent.

The order of the reaction and the rate constant value can find out from the kinetics adsorption data. The adsorptive removal of B ions from aqueous solution on the adsorbent can be explained on the basis of kinetics models and the observed rate controlling mechanism of adsorption processes such as chemical reaction, diffusion control, and mass transfer. The kinetic of B adsorption onto CuO NPs was evaluated by three models, viz. pseudo-first-order, pseudo-second-order, and intraparticle diffusion models, and the results are given in Tables 1 and 4. The pseudo-first-order equation assumes that the bindings originate from physical adsorption based on the equation given in Table 1. The pseudo-second-order model gives chemical adsorption (chemisorption) and the equation is given in Table 1. In addition to this, the intraparticle diffusion model was applied to identify the diffusion mechanism. The equation of the intraparticle diffusion model is given in Table 1.

In this equation, q_e and q_t (mg/g) are the adsorption capacity of CuO NPs at equilibrium and at time t (min), respectively. k_1 (per min) and k_2 (g/mg/min) are the pseudo-first-order and pseudo-second-order rate constant values, respectively. The k_i (mg/g/min$^{0.5}$) and C are the intraparticle diffusion rate constant and intercept, respectively. Only the kinetics model constant of pseudo-second-order is represented in Table 4 because the correlation coefficient of other models was less than 0.6000. Therefore, the kinetics results indicate that the adsorption of B ions is controlled by the pseudo-second-order model (R^2 = 0.9688) rather than the pseudo-first-order (R^2 = 0.5671) and intraparticle diffusion (R^2 = 0.0697) models, indicating that the adsorption process of B ions occurs due to the chemisorption [9]. The assumption behind the pseudo-second-order model

Table 3
Thermodynamics parameters for the B ions adsorption onto CuO NPs

CuO NPs				
Temperature (°C)	lnK_c	$\Delta G°$ (kJ/mol)	$\Delta H°$ (kJ/mol)	$\Delta S°$ (J/mol/K)
15	6.3	–15.27		
20	6.3	–15.53		
25	6.7	–16.71	+10.7	+90.4
30	6.5	–16.62		
35	6.7	–17.21		
40	6.0	–17.80		

Table 4
Kinetic parameters of the pseudo-second-order model for boron adsorption on CuO NPs at 25°C, initial boron concentration 10 mg/L

Parameters of kinetic models	CuO
R^2	0.968
k_2	0.07
q_e	3.5

is that the rate-limiting step may be the chemisorption involving valence forces through the sharing or exchange of electrons between the adsorbent and the adsorbate. This mechanism was in accordance with the mechanism proposed in the section on pH.

3.4. Boron adsorption isotherms in non-competitive and competitive solutions

The results of the B adsorption in non-competitive and competitive equilibrium experiments for CuO NPs as the adsorbent are given in Fig. 7. At a pH level of 7, a part of B exists in the form of H_3BO_3. On the other hand, the PZC, which gives an estimated measure of the surface charges, was positive for this pH values (Table 2). Thus, the adsorption of B took place via chemisorption. In this study, four isotherms models, including Langmuir, Freundlich, Temkin, and Dubinin–Radushkevich (D–R), were applied to understand the adsorption mechanism. The linear and non-linear forms of the studied models are given in equations of Table 1 [34]. In these equations, C_e (mg/L) is the adsorbate concentration at equilibrium in solution, q_e (mg/g) is the amount of metal ions adsorbed onto adsorbent, q_{max} (mg/g) is maximum monolayer adsorption capacity, and b (L/mg) is the Langmuir constant related to the affinity of binding sites. K_F (mg/g(L/mg)$^{1/n}$) is the Freundlich constant, and n is the heterogeneity factor related to the intensity of adsorption. B (J/mol) is the Temkin constant related to the heat of adsorption, R (8.314 J/mol K) is the gas constant, T (K) is absolute temperature, K_T (L/g) is the equilibrium binding constant, and q_m (mg/g) is the maximum adsorption capacity. β is the activity coefficient related to sorption mean free energy (mol^2/kJ^2), ε is Polanyi potential, and E (kJ/mol) is the mean adsorption energy, which was calculated from Eqs. (6) and (7), respectively.

$$\varepsilon = RT\ln\left(1+\frac{1}{C_e}\right) \tag{6}$$

$$E = \frac{1}{\sqrt{-2\beta}} \tag{7}$$

If E is less than 20 kJ/mol, the adsorption proceeds by weak van der Waals forces. The energy for chemisorption lies in the range of 40–800 kJ/mol. Table 5 compares the fitting of the experimental data with Langmuir, Freundlich, D–R, and Temkin adsorption isotherms. The Langmuir model assumes monolayer adsorption of ions on the adsorbent surface and indicates that the adsorption

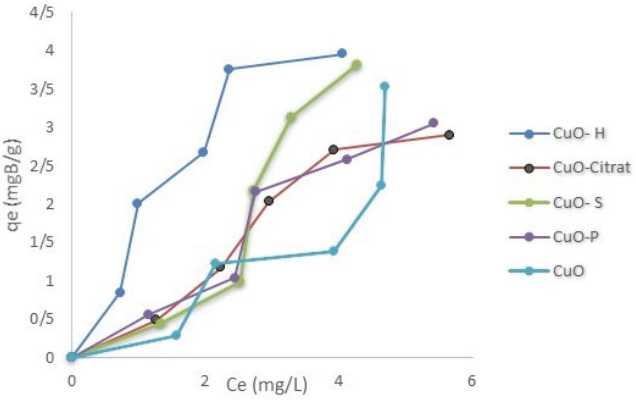

Fig. 7. Adsorption isotherms of boron in non-competitive and competitive (with humic, citrate, sulfate, and phosphate) solutions.

is chemisorption. As mentioned in Table 5, sorption data did not fit the Langmuir model because of a low correlation coefficient (R^2 < 0.5219). Freundlich model is an empirical equation used in adsorptions on heterogeneous surfaces [12]. The Dubinin–Radushkevich (D–R) isotherm is more common than the above two models as it rejects the homogeneous surface or constant adsorption potential. It is observed that the Freundlich model, and in the next stages D–R and Temkin models with average correlation coefficients (R^2) of 0.9621, 0.9137, and 0.9028, respectively, were more suitable in simulating the adsorption isotherm of B onto CuO NPs. The related parameters are also summarized in Table 5. The effects of side ions (competitive anions), which are present in natural waters, on B removal were evaluated in the presence of humate, phosphate, sulfate, and citrate over a concentration range of 0–10 mg/L. As can be seen in Fig. 7, there is no essential effects of side salt ions on B removal even at their high contents in water. These data prove the highly specific B sorption with CuO NPs from multi-component aqueous solutions. A similar result was reported previously on high selectivity of CuO when used for B removal from complex solutions [6]. Comparisons of adsorption properties of the current CuO NPs with other adsorbents are very difficult because of dissimilar applied experimental conditions. Table 6 compares the adsorption capacities of different adsorbents for B adsorption reported in the literature and in this research, indicating the highest B adsorption capacity of CuO compared to other adsorbents such as activated carbon.

3.5. SEM-EDX studies after competitive and non-competitive isotherms

In order to investigate the morphological changes of the nano-adsorbent surfaces, SEM-EDX samples were taken after the application of B treatment (Fig. 8). Results revealed that the surface of the particles was smoother before the treatment than after the operation. Such a change in the particle surface indicates that the adsorption is due to boron because of low concentrations of equilibrium solutions (C_e) in the isotherm; hence it can be inferred that the removal of B took place via specific adsorption (chemisorption).

Table 5
Boron adsorption parameters calculated by Langmuir, Temkin, and Freundlich isotherm

Freundlich isotherm	R^2	n	K_F	Adsorption capacity*
CuO	0.965	0.4	1.4	3.5
CuO-S	0.963	0.5	4.1	3.5
CuO-Citrate	0.986	0.6	2.3	2.8
CuO-P	0.966	0.8	2.0	3.0
CuO-H	0.9304	1.2	1.6	3.0
Temkin isotherm	R^2	K_T	B	
CuO	0.8637	1.6918	0.5915	
CuO-S	0.7951	2.663	0.6295	
CuO-citrate	0.9499	1.8928	0.6928	
CuO-P	0.9136	1.7618	0.7333	
CuO-H	0.9918	2.1434	1.4122	
Langmuir isotherm	R^2	q_{max}	K_L	
CuO	0.4700	15.69	0.031	
CuO-S	0.9181	1.667	0.1930	
CuO-citrate	0.3986	5.23	0.0845	
CuO-P	0.3009	6.93	0.0684	
CuO-H	0.0763	–	–	
D–R	R^2	q_m	E	
CuO	0.9805	3.54	0.707	
CuO-S	0.8379	4.3	1.00	
CuO-citrate	0.9663	3.26	1.054	
CuO-P	0.8443	2.91	1.195	
CuO-H	0.9394	4.47	1.825	

*adsorption capacity calculated from the final points of isotherms.

Table 6
Comparison of adsorption capacities of materials used for the removal of boron

Adsorbent	pH	Sorption capacity (mg/g)	Ref.
Goethite	8.2	0.3	[35]
Vermiculite	9.2	1.62	[36]
Activated carbon (AC)	–	0.014	[9]
Fly ash agglomerates	10–10.5	0.014	[37]
Natural geologic material	–	0.0023	[38]
Partly-weathered volcanic ash	–	0.085	[39]
Calcined magnesite tailing	6	0.085	–
CuO	7	3.5	This study
CuO-S	7	3.5	This study
CUO-C	7	2.8	This study
CUO-P	7	3.0	This study
CuO-H	7	3.0	This study

EDX analysis was also performed to ensure greater adsorption, and the results (Fig. 9) show the sorption of B and coexisting anions in each analysis performed in both non-competitive and competitive isotherms. As shown in Fig. 9, boron, humates, sulfates, and citrates are adsorbed on CuO NPs.

3.6. Desorption studies

In an effective removal process, ions adsorbed by the adsorbent should not be easily desorbed into the environment. In CuO NPs, the reaction of particle surfaces with the pollutants should be irreversible because the unstable

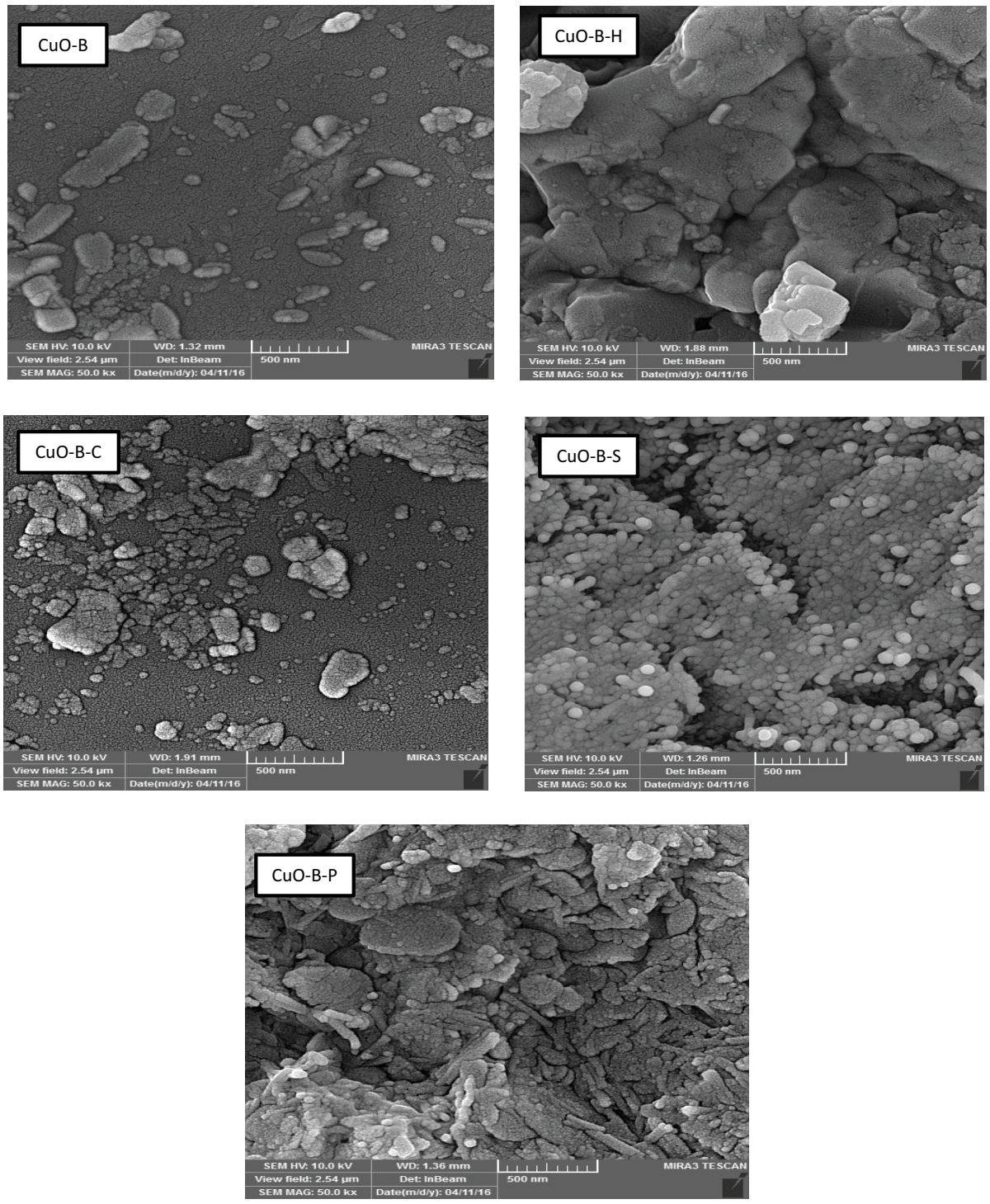

Fig. 8. SEM images of CuO NPs after boron adsorption on two simple and competitive (with humic, citrate, sulfate, and phosphate anions) isotherms.

reaction in the aqueous and soil environments may desorb the pollutants and bring them into the environment. Accordingly, the amounts of desorption were 3.4%, 33.3%, 13.2%, 9.9%, and 16.7% in simple and competitive isotherms for phosphate, citrate, humate, and sulfate anions, respectively, in an initial concentration of 2 mg/L for B (initial point of isotherm) (Fig. 10). Our results indicate that the boron-loaded sorbent cannot be effectively desorbed and regenerated via $CaCl_2$ treatment. Therefore, with respect to the pH_{PZC} value of CuO NPs, kinetic results, and low desorption results, it seems that chemisorption is the dominant mechanism of B sorption on CuO NPs.

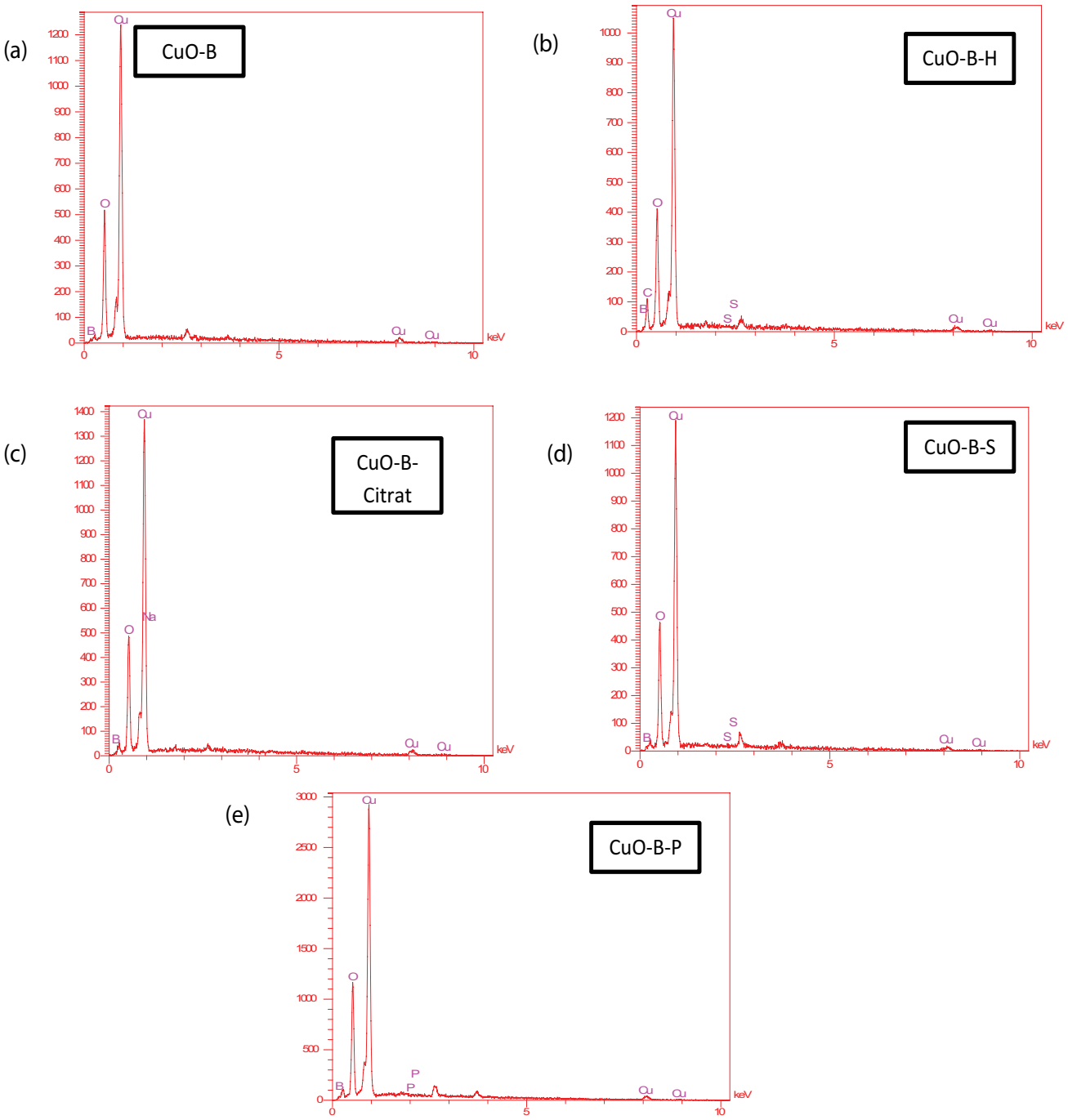

Fig. 9. EDX images of CuO NPs after boron adsorption on two simple and competitive (with humic, citrate, sulfate, and phosphate anions) isotherms.

4. Conclusions

This study presents information obtained by CuO NPs and their use in B removal from water. The ability of B removal from the solution to the adsorbent and then recovery of the adsorbent for reuse were demonstrated by our findings. SEM analysis showed that the CuO NPs were nanostructured aggregates. The kinetics tests indicated that the B sorption on CuO obeyed the pseudo-second-order kinetics. Thermodynamics and kinetics experiments revealed that the nature of B sorption was spontaneous and endothermic. The adsorption isotherm followed the Freundlich isotherm model and B sorption capacity was 3.5 mg/g in non-competitive solution at equilibrium for an initial B concentration of 10 mg/L. CuO NPs saturated with B were found to be efficiently retained after treatment

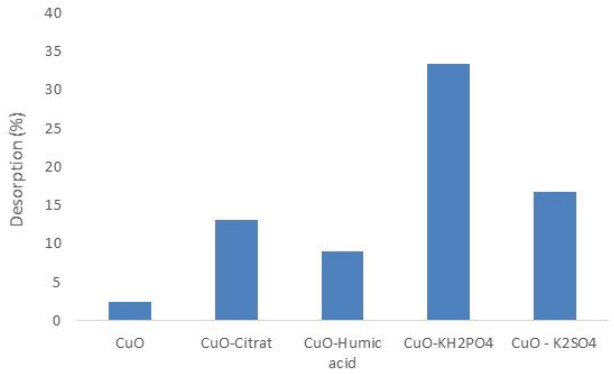

Fig. 10. Desorption experiments in initial point isotherms in non-competitive and competitive solutions (C_0 = 2 mg/L).

with $CaCl_2$ (0.01 M). Therefore, the CuO NPs demonstrated to be excellent candidates for the removal of B ions from non-competitive and competitive solutions.

References

[1] M. Tagliabue, A.P. Reverberi, R. Bagatin, Boron removal from water: needs, challenges, and perspectives, J. Cleaner Prod., 77 (2014) 56–64.

[2] M.A. Al-Ghouti, N.R. Salih, Application of eggshell wastes for boron remediation from water, J. Mol. Liq., 256 (2018) 599–610.

[3] Z. Guan, J. Lv, P. Bai, X. Guo, Boron removal from aqueous solutions by adsorption—a review, Desalination, 383 (2016) 29–37.

[4] O.C. Türker, J. Vymazal, C. Türe, Constructed wetlands for boron removal: a review, Ecol. Eng., 64 (2014) 350–359.

[5] M.Al. Haddabi, M. Ahmed, Z.Al. Jebri, H. Vuthaluru, H. Znad, M.Al. Kindi, Boron removal from seawater using date palm (*Phoenix dactylifera*) seed ash, Desal. Water Treat., 57 (2016) 5130–5137.

[6] G. Zelmanov, R. Semiat, Boron removal from water and its recovery using iron (Fe^{+3}) oxide/hydroxide-based nanoparticles (NanoFe) and NanoFe-impregnated granular activated carbon as adsorbent, Desalination, 333 (2014) 107–117.

[7] M. Bodzek, The removal of boron from the aquatic environment–state of the art, Desal. Water Treat., 57 (2016) 1107–1131.

[8] J. Wolska, M. Bryjak, Methods for boron removal from aqueous solutions—a review, Desalination, 310 (2013) 18–24.

[9] V. Masindi, M.W. Gitari, H. Tutu, M. Debeer, Removal of boron from aqueous solution using magnesite and bentonite clay-composite, Desal. Water Treat., 57 (2016) 8754–8764.

[10] T. Chen, Q. Wang, J. Lyu, P. Bai, X. Guo, Boron removal and reclamation by magnetic magnetite (Fe_3O_4) nanoparticle: an adsorption and isotopic separation study, Sep. Purif. Technol., 231 (2020) 115930.

[11] J. Kluczka, W. Pudło, K. Krukiewicz, Boron adsorption removal by commercial and modified activated carbons, Chem. Eng. Res. Des., 147 (2019) 30–42.

[12] S. Yu, H. Xue, Y. Fan, R. Shi, Synthesis, characterization of salicylic-HCHO polymeric resin and its evaluation as a boron adsorbent, Chem. Eng. J., 219 (2013) 327–334.

[13] E. Babiker, M.A. Al-Ghouti, N. Zouari, G. McKay, Removal of boron from water using adsorbents derived from waste tire rubber, J. Environ. Chem. Eng., 7 (2019) 102948.

[14] I. Mohmood, C.B. Lopes, I. Lopes, I. Ahmad, A.C. Duarte, E. Pereira, Nanoscale materials and their use in water contaminants removal—a review, Environ. Sci. Pollut. Res., 20 (2013) 1239–1260.

[15] S. Mahdavi, D. Akhzari, The removal of phosphate from aqueous solutions using two nano-structures: copper oxide and carbon tubes, Clean Technol. Environ Policy, 18 (2016) 817–827.

[16] S. Mahdavi, P. Molodi, M. Zarabi, Functionalized MgO, CeO_2 and ZnO nanoparticles with humic acid for the study of nitrate adsorption efficiency from water, Res. Chem. Intermed., 44 (2018) 543–562.

[17] M. Verma, I. Tyagi, R. Chandra, V.K. Gupta, Adsorptive removal of Pb(II) ions from aqueous solution using CuO nanoparticles synthesized by sputtering method, J. Mol. Liq., 225 (2017) 936–944.

[18] S. Mahdavi, M. Jalali, A. Afkhami, Removal of heavy metals from aqueous solutions using Fe_3O_4, ZnO, and CuO nanoparticles, J. Nanopart. Res., 14 (2012) 171–188.

[19] A. Chakraborty, D.A. Islam, H. Acharya, Facile synthesis of CuO nanoparticles deposited zeolitic imidazolate frameworks (ZIF-8) for efficient photocatalytic dye degradation, J. Solid State Chem., 269 (2019) 566–574.

[20] J.W. Kim, C.S. Ki, I.C. Um, Y.H. Park, A facile fabrication method and the boosted adsorption and photodegradation activity of CuO nanoparticles synthesized using a silk fibroin template, J. Ind. Eng. Chem., 56 (2017) 335–341.

[21] V.K. Gupta, R. Chandra, I. Tyagi, M. Verma, Removal of hexavalent chromium ions using CuO nanoparticles for water purification applications, J. Colloid Interface Sci., 478 (2016) 54–62.

[22] P. Nuengmatcha, P. Porrawatkul, S. Chanthai, P. Sricharoen, N. Limchoowong, Enhanced photocatalytic degradation of Methylene blue using Fe_2O_3/graphene/CuO nanocomposites under visible light, J. Environ. Chem. Eng., 7 (2019) 103438.

[23] I. Jacukowicz-Sobala, D. Ociński, P. Mazur, E. Stanisławska, E. Kociołek-Balawejder, Evaluation of hybrid anion exchanger containing cupric oxide for As(III) removal from water, J. Hazard. Mater., 370 (2019) 117–125.

[24] D.L. Sparks, A. Le Page, P.A. Helmke, R.H. Loeppert, P.N. Soltanpour, M.A. Tabatabai, C.T. Johnston, M.E. Sumner, Methods of Soil Analysis. Part 3-Chemical Methods, Soil Science Society of America Inc., Madison, Wis., 1996.

[25] S. Mahdavi, N. Amini, The role of bare and modified nano nickel oxide as efficient adsorbents for the removal of Cd^{2+}, Cu^{2+}, and Ni^{2+} from aqueous solution, Environ. Earth Sci., 75 (2016) 1468.

[26] S. Mahdavi, N. Amini, H. Merrikhpour, D. Akhzari, Characterization of bare and modified nano-zirconium oxide (ZrO_2) and their applications as adsorbents for the removal of bivalent heavy metals, Korean J. Chem. Eng., 34 (2017) 234–244.

[27] H.K. Moghaddam, M. Pakizeh, Experimental study on mercury ions removal from aqueous solution by MnO_2/CNTs nanocomposite adsorbent, J. Ind. Eng. Chem., 21 (2015) 221–229.

[28] V.V.T. Padil, M. Černík, Green synthesis of copper oxide nanoparticles using gum karaya as a biotemplate and their antibacterial application, Int. J. Nanomed., 8 (2013) 889.

[29] O.C. Türker, T. Baran. Evaluation and application of an innovative method based on various chitosan composites and *Lemna gibba* for boron removal from drinking water, Carbohydr. Polym., 166 (2017) 209–218.

[30] N.B. Darwish, V. Kochkodan, N. Hilal, Boron removal from water with fractionized amberlite IRA743 resin, Desalination, 370 (2015) 1–6.

[31] A. Kurniawan, S. Ismadji. Potential utilization of *Jatropha curcas* L. press-cake residue as new precursor for activated carbon preparation: application in Methylene blue removal from aqueous solution, J. Taiwan Inst. Chem. Eng., 42 (2011) 826–836.

[32] S.K. Theydan, M.J. Ahmed, Adsorption of Methylene blue onto biomass-based activated carbon by $FeCl_3$ activation: equilibrium, kinetics, and thermodynamic studies, J. Anal. Appl. Pyrolysis, 97 (2012) 116–122.

[33] J. Lyu, N. Zhang, H. Liu, Z. Zeng, J. Zhang, P. Bai, X. Guo, Adsorptive removal of boron by zeolitic imidazolate framework: kinetics, isotherms, thermodynamics, mechanism, and recycling, Sep. Purif. Technol., 187 (2017) 67–75.

[34] N. Kataria, V. Garg, Optimization of Pb(II) and Cd(II) adsorption onto ZnO nanoflowers using central composites design: isotherms and kinetics modeling, J. Mol. Liq., 271 (2018) 228–239.

[35] E. Goli, R. Rahnemaie, T. Hiemstra, M.J. Malakouti, The interaction of boron with goethite: experiments and CD–MUSIC modelling, Chemosphere, 82 (2011) 1475–1481.
[36] M. Kehal, L. Reinert, L. Duclaux, Characterization and boron adsorption capacity of vermiculite modified by thermal shock or H_2O_2 reaction and/or sonication, Appl. Clay Sci., 48 (2010) 561–568.
[37] S. Seyhan, Y. Seki, M. Yurdakoc, M. Merdivan, Application of iron-rich natural clays in Camlica, Turkey for boron sorption from water and its determination by fluorimetric-azomethine-H method, J. Hazard. Mater., 146 (2007) 180–185.
[38] C.B. Tabelin, T. Igarashi, T. Arima, D. Sato, T. Tatsuhara, S. Tamoto, Characterization and evaluation of arsenic and boron adsorption onto natural geologic materials, and their application in the disposal of excavated altered rock, Geoderma, 213 (2014) 163–172.
[39] İ. Kıpçak, M. Özdemir, Removal of boron from aqueous solution using calcined magnesite tailing, Chem. Eng. J., 189 (2012) 68–74.